Research Article Vol. 33, No. 26 / 29 Dec 2025 / Optics Express 54275
Optics EXPRESS

Measurement of elastic properties of optical fibers under hydrogen and deuterium diffusion by forward-stimulated Brillouin scattering

A. S. Paterno,[1,2,*] C. Álvarez-Ocampo,[1] A. Díez,[1,3] M. Delgado-Pinar,[1,3] J. L. Cruz,[1,3] and M. V. Andrés[1,3]

[1]Laboratory of Fiber Optics, ICMUV, Universidad de Valencia, Burjassot, Spain
[2]Department of Electrical Engineering, CCT - UDESC, Center for Science and Technology, Santa Catarina State University, Joinville, Santa Catarina, Brazil
[3]Departamento de Física Aplicada y Electromagnetismo, Universidad de Valencia, Burjassot, Spain
*aleksander.paterno@udesc.br

Abstract: The hydrogen and deuterium diffusion process in standard single-mode silica optical fibers was investigated using forward-stimulated Brillouin scattering. The method relies on the sensitivity of the resonance frequency of the transverse acoustic modes of the fiber to changes in the fiber's elastic properties. We developed a pump-and-probe experiment to stimulate and interrogate a large number of transverse acoustic modes in a short section of fiber undergoing gas loading at high pressure, followed by outdiffusion. The shift in resonance frequencies was monitored throughout the process. Thus, the temporal dynamics of gas diffusion were investigated. The changes in the two acoustic velocities —shear and longitudinal— and in Poisson's ratio resulting from gas diffusion were obtained. For an estimated hydrogen concentration of 0.57 mol.%, a change of 0.96 m/s and 2.46 m/s was measured in the shear and longitudinal acoustic velocities, respectively, and a change in the Poisson's ratio of 1.6×10^{-4}.

1. Introduction

The effects of the presence of hydrogen and deuterium on silica have been thoroughly investigated in the context of optical fibers. Various fundamental studies have highlighted the impact of the diffusion of these gases on the optical and mechanical properties of optical fibers [1–4]. Exposure of fibers to hydrogen results in increased fiber attenuation in the transmission window, and hydrogen molecules in the glass network have also been shown to negatively affect pump efficiency in rare-earth-doped fiber lasers and amplifiers [5]. In the field of fiber optic sensors, hydrogen diffusion affects both Raman-based distributed sensors [6] and backward Brillouin scattering (BBS)-based sensors [7,8]. In the latter case, the hydrogen content modifies Brillouin scattering in two ways: it reduces the gain amplitude and shifts the Brillouin frequency. In particular, the frequency shift is partially due to the change in the fiber's elastic properties [9]. However, several applications benefit from changes in the physicochemical properties of optical fibers caused by the presence of hydrogen or deuterium. Kong and Dong [10] demonstrated that, in combination with UV irradiation, hydrogen diffusion can be used to modify and partially suppress the Brillouin gain in telecommunication fibers. Moreover, hydrogen (or deuterium) loading is used for Bragg gratings writing in fibers, as it significantly improves the formation of gratings in Ge-doped silica core fibers upon UV irradiation [11,12].

In this work, we report the use of forward-stimulated Brillouin scattering (FSBS) for investigating the effects of the diffusion of hydrogen and deuterium on the elastic properties of single-mode optical fibers. FSBS involves the interplay of two copropagating optical waves and a nearly transverse acoustic mode [13]. In recent years, many interesting applications based on FSBS have been demonstrated [14–19]. FSBS is strongly dependent on the geometric and the elastic

#580774 https://doi.org/10.1364/OE.580774
Journal © 2025 Received 2 Oct 2025; revised 23 Nov 2025; accepted 25 Nov 2025; published 18 Dec 2025

Optics EXPRESS

properties of the optical fiber, making it an effective mechanism for the accurate characterization of optical fibers. Notable results in this regard include the measurement of the Poisson ratio in optical fibers with unparalleled accuracy [20], the characterization of the elastic properties of fiber coatings [21], and the analysis of the fiber diameter with nanometer resolution [22,23]. By this method, we investigated how the mechanical properties of the optical fiber change due to the diffusion of H_2 or D_2, as well as its temporal dynamics. The method benefits from the high Q factor (>5000) of the FSBS gain peaks. The multi-peak response of FSBS contributes to improved accuracy, as it allows linear fitting procedures to be used to obtain the results.

The variation of the longitudinal acoustic velocity (v_L) in H_2-loaded optical fibers was previously studied using BBS [9]. BBS involves only one acoustic mode—the fundamental longitudinal acoustic mode. However, the variety of acoustic modes that can be stimulated by FSBS, with different properties, allowed us to extend previous reports and to investigate the impact of H_2 and D_2 diffusion on both acoustic velocities, longitudinal (v_L) and shear (v_S), and on the Poisson's ratio of the optical fiber. In addition, FSBS permits to monitor the diffusion from the beginning of the process, since the acoustic field expands over the whole fiber cross section, while BBS only detects the presence of the gas when it reaches the core of the fiber. In a potential sensing application for hydrogen detection, early detection is critically important since hydrogen is highly flammable and requires very little energy to ignite.

The proposed technique complements the classical optical methods to analyze hydrogen and deuterium diffusion in optical fibers, as in monitoring attenuation at specific wavelengths [2] and measuring changes in the core refractive index [24–26], which in fact do not monitor the beginning of the diffusion process.

2. Fundamentals

In single-mode optical fibers, two types of transverse acoustic modes can be optically stimulated through FSBS: pure radial acoustic modes $R_{0,m}$, and torsional radial modes of angular order $n = 2$, $TR_{2,m}$ [13]. Phase-matching is fulfilled for acoustic modes close to their cutoff frequency. The study reported in this paper is based on the response of torsional-radial $TR_{2,m}$ modes. $TR_{2,m}$ modes exhibit transverse displacement vector profiles with two-fold azimuthal symmetry. Strictly speaking, the displacement vector of the $TR_{2,m}$ acoustic modes comprises both, an angular (shear) component and a radial (dilatational) component. However, particularly for high-order modes, it has been shown that $TR_{2,m}$ modes exhibit either a strong shear character, with a field dominated by the angular term, or a dilatational character, with a field dominated by the radial term [20,28]. We denote these as ${TR_{2,m}}^{(1)}$ and ${TR_{2,m}}^{(2)}$, respectively. Their cutoff frequency can be approximated by [20]:

$$\Omega_{2,m}^{(1)} \approx \frac{v_S}{a}\left(c_{m+1} - \frac{15}{8 \cdot c_{m+1}}\right) \tag{1}$$

$$\Omega_{2,m}^{(2)} \approx \frac{v_L}{a}\left(c_{m+1} - \frac{15}{8 \cdot c_{m+1}}\right) \tag{2}$$

where $c_m = m\pi - \pi/4$, with m being an integer number that denotes the mode order, a is the fiber radius and v_S and v_L are the shear and longitudinal acoustic velocities, respectively. The second term within the parentheses in Eq. (1) and (2) quickly tends to zero with increasing mode order. Thus, the frequency is nearly linear with respect to the mode order in both cases, with slopes proportional to v_S and v_L, respectively.

The diffusion of hydrogen or deuterium in the silica matrix modifies the mechanical properties of the optical fiber, which in turn affects the acoustic velocities [29]. Under the pressure and temperature conditions of the experiments, the diffusion proceeds interstitially with no significant chemical interaction with the host material [1,3,25]. H_2 and D_2 molecules are trapped singly in interstitial sites in silica [2].

Optics EXPRESS

According to Eq. (1) and (2), a change in the acoustic velocities leads to the frequency shift of the FSBS acoustic modes. Therefore, by measuring the frequency shift of both types of $TR_{2,m}$ acoustic modes, the effects of gas diffusion on the two acoustic velocities and, by extension, on the Poisson's ratio can be derived. Moreover, while each mode will undergo a specific amount of shift, the relative frequency shift, $\Delta\Omega/\Omega$, will remain constant for all modes of the same sub-type. This approach enabled us to implement averaging strategies or linear fitting procedures to obtain the results, thereby reducing uncertainty.

Radial modes are also sensitive to changes in the mechanical properties of the fiber. Therefore, diffusion of H_2 or D_2 into the fiber can be investigated with $R_{0,m}$ acoustic modes. Their cut-off frequency is nearly proportional to v_L [20], thus, changes in v_L can also be obtained from radial acoustic modes.

It is worth to note that the cutoff frequency of FSBS acoustic modes depends only on the mechanical properties of the optical fiber, not on its optical properties. Therefore, changes in acoustic properties can be directly obtained from FSBS. It is not necessary to know the variation in optical properties that also occurs in the optical fiber due to H_2 or D_2 diffusion to obtain changes in the acoustic properties. This approach differs from techniques based on backward Brillouin scattering in which the frequency shift results from the superposition of both mechanical and optical properties. In [9], the increase in the longitudinal acoustic velocity in optical fibers with H_2 concentration was determined by the combination of backward Brillouin scattering and Rayleigh scattering measurements. The latter were performed to determine the variation in refractive index that was required to work out the longitudinal acoustic velocity variation from Brillouin scattering measurements. On the other hand, backward Brillouin scattering does not provide information about shear acoustic velocity.

Acoustic velocities are determined by Young's modulus E, the density of the material ρ, and the Poisson's ratio ν as [29]:

$$v_L = \sqrt{\frac{E(1-\nu)}{\rho(1+\nu)(1-2\nu)}} \tag{3}$$

$$v_S = \sqrt{\frac{E}{2\rho(1+\nu)}} \tag{4}$$

The presence of H_2 or D_2 can affect all elastic and geometric parameters. When those changes are homogeneous over the optical fiber cross-section, which is a reasonable assumption at saturation, the relative frequency shift can be expressed as follows:

$$\frac{\Delta\Omega^{(i)}}{\Omega^{(i)}} = -\frac{\Delta a}{a} - \frac{1}{2}\frac{\Delta\rho}{\rho} + \frac{1}{2}\frac{\Delta E}{E} + C^{(i)}\Delta\nu \tag{5}$$

where $i = 1, 2$ denotes the sub-type of $TR_{2,m}$ acoustic mode, Δa is the change in the radius of the fiber, $\Delta\rho$ is the change in density, and ΔE and $\Delta\nu$ are the change in Young's modulus and Poisson's ratio, respectively. The coefficients $C^{(i)}$ depend on the Poisson ratio, taking the values $C^{(1)} = -0.43$ and $C^{(2)} = 0.50$ for $\nu = 0.174$ [20]. It is important to note that the only term in Eq. (5) that differs for shear-like and dilatation-like $TR_{2,m}$ modes is the one that concerns the change in Poisson's ratio.

3. Experimental aspects

3.1. Experimental setup

Figure 1 illustrates the experimental setup that uses a pump-probe configuration. The FSBS acoustic modes were optically stimulated using a pulsed Nd-YAG microchip laser operating at 1064 nm. The laser emitted linearly polarized pulses of duration 700 ps with a repetition rate of

Optics EXPRESS

19 kHz and pulse energy of 7 μJ. The oscillation of acoustic modes was probed using a linearly polarized CW tunable laser diode that emits at 1550 nm, with a 10 kHz linewidth and 6.25 mW optical power. The polarization state of the pump and probe waves was adjusted using a set of waveplates and a fiber polarization controller, respectively.

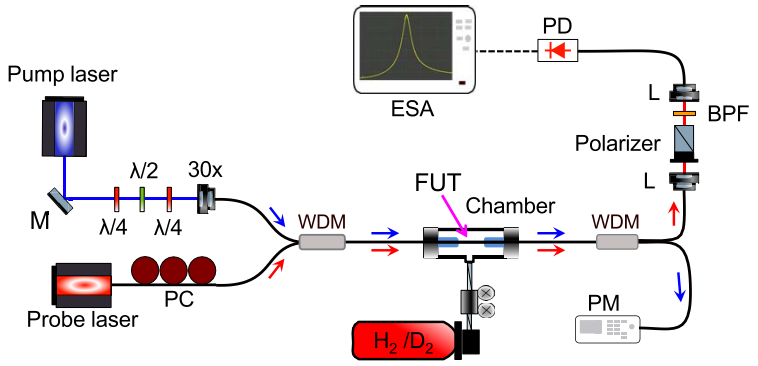

Fig. 1. Experimental setup for hydrogen or deuterium diffusion monitoring. FUT: fiber under test; PC: polarization controller; PD: photodiode; BPF: band-pass filter; L: collimation lens; PM: power meter; WDM: wavelength-division multiplexer; ESA: electric spectrum analyzer.

The fiber under test consisted of a section of 25 cm of Corning SMF-28 fiber with its coating removed. Pump and probe waves were delivered to the FUT through a 1064 nm/1550 nm wavelength-division multiplexer (WDM) fiber coupler that was fusion spliced to the FUT. The pump wave leakage at the output port of the WDM was photodetected and used as the trigger signal for the oscilloscope. A second WDM was spliced at the output end of the FUT to remove the pump. The polarization modulation of the probe wave resulting from the oscillation of the acoustic modes was converted into and intensity modulated signal using a Glan-Thompson linear polarizer. This modulation was then photodetected and acquired using an oscilloscope and an electrical spectrum analyzer (ESA). The FUT was placed inside a sealed chamber, into which hydrogen or deuterium was injected through an inlet. Pressure was monitored during the experiment with a digital pressure gauge with an absolute error of 0.3 bar. The temperature of the chamber was precisely controlled and kept within a range $\pm$ 0.1°C during the measurement sequence.

3.2. Measurement procedure

Experiments were performed with hydrogen and deuterium. A different section of fiber was used in each experiment. For each gas, the FUT underwent a complete cycle of gas loading (reaching saturation) and complete outdiffusion. Hydrogen or deuterium was introduced into the chamber at a controlled pressure of 50 bar and 23°C. According to [11,25], the estimated concentration of H_2/D_2 in the fiber at saturation was 0.57 mol. %. The FSBS spectrum of a number of $TR_{2,m}$ acoustic modes of both sub-types, with resonance frequency ranging from 108 MHz to 560 MHz, were recorded at different instants during the cycle. The spectrum of each resonance was acquired with 100 averages. The acquisition time for all measured modes was in the order of a few minutes. The time interval between two consecutive measurements was adapted to the response. For instance, during the initial phases of loading and degassing, when rapid changes were observed, data were collected at two-hour intervals. However, near saturation or complete outdiffusion, data were collected every 24 hours. The peaks in the spectrum exhibited a SNR > 30 dB. The resonance frequency of each acoustic mode was subsequently obtained after fitting a Breit-Wigner-Fano model [30] to the acquired spectra.

Optics EXPRESS

4. Experimental results

Figure 2 presents the spectrum corresponding to $TR^{(2)}_{2,6}$ acoustic mode at five pertinent times in the loading/outdiffusion cycle, that is, (1) before gas pressure was applied, (2) immediately after gas pressure was applied, (3) at saturation, (4) immediately after gas pressure was released and (5) when the outdiffusion was complete. This particular case corresponds to the experiment with deuterium. When deuterium pressure was applied to the fiber, the peak shifted to a lower frequency. This phenomenon is merely a consequence of the pressure and does not have a relation to the diffusion of the gas into the fiber. The study of the effect of pressure on FSBS is beyond the scope of this paper and will be analyzed elsewhere. The pressure-induced frequency shift remained constant during the gas loading stage, as the pressure was maintained constant at 50 bar. A shift of the peak towards higher frequencies was observed during the D_2 loading stage. Figure 2(b) shows the spectrum at the beginning of the gas loading stage and at saturation. When pressure was released, the initial negative shift induced when pressure was applied was reversed, as can be seen in Fig. 2(c). A net positive shift of 101 kHz was observed between the pristine fiber as in Fig. 2(b) and the D_2-saturated fiber for this specific acoustic mode. Finally, during the outdiffusion stage, the peak shifted towards lower frequencies until the gas outdiffusion was complete, and the initial spectrum was recovered. No measurable broadening of the spectra was observed, which could indicate that the presence of deuterium in the fiber does not have a noticeable impact on acoustic attenuation. Similar qualitative behavior to that shown in Fig. 2 was observed in other acoustic modes, and when the fiber was exposed to H_2.

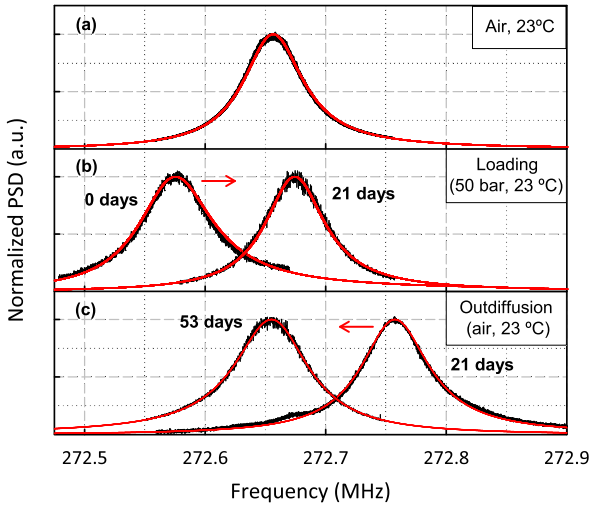

Fig. 2. Normalized power spectral density (PSD) corresponding to the $TR^{(2)}_{2,6}$ acoustic mode during D_2 diffusion experiments at 23°C. (a) Before starting the process; (b) just after gas pressure was applied (0 days) and after 21 days of D_2 loading at 50 bar; (c) just after releasing the gas pressure (21 days) and after complete gas outdiffusion (53 days). Black lines show the raw data while red lines show the best fit.

Figure 3(a) shows the resonance frequencies of the modes measured in this work as a function of the mode order. Empty dots indicate specific $TR_{2,\mathrm{m}}$ modes whose response is not well described by Eq. (1) and (2), as their displacement fields contain both dilatational and shear components of comparable amplitude. This happens when a $TR^{(1)}_{2,m}$ mode and a $TR^{(2)}_{2,m}$ mode are quasi-degenerated. Those modes were not considered for further calculations. Note that mixed-type modes can be of interest because of their different response from that of dilatational-type and shear-type modes, which could eventually be exploited to perform simultaneous and discriminative measurement of

Optics EXPRESS

different magnitudes. Acoustic modes with mode order lower than 4 were excluded because they exhibit a strong mixed-type behavior [28]. Acoustic modes with mode order beyond 15 were not considered as the signal-to-noise ratio of the peaks was not good enough to obtain the resonance frequency with enough accuracy.

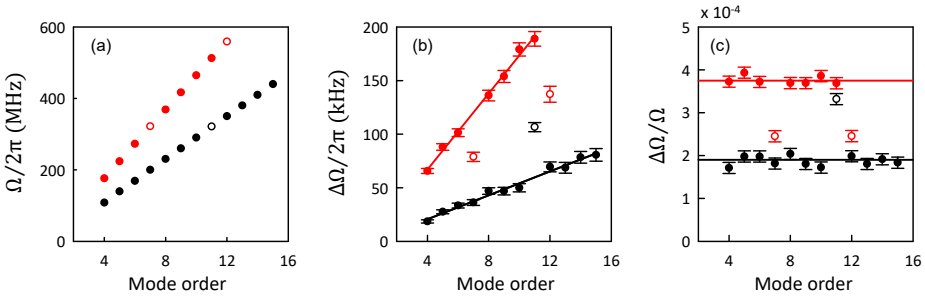

Fig. 3. (a) Frequency of the $TR_{2,m}$ acoustic modes measured in this work as a function of mode order. (b) Frequency shift and (c) relative frequency shift of $TR_{2,m}$ acoustic modes at saturation with respect to the pristine fiber. $TR^{(1)}_{2,m}$ are shown in black and $TR^{(2)}_{2,m}$ in red. Empty symbols indicate modes with strong mixed character.

The frequency shift and relative frequency shift that they experienced when the fiber was saturated with deuterium is shown in Fig. 3(b) and 3(c). As shown in Fig. 3(c), most of the acquired acoustic modes of a given series – $TR^{(1)}_{2,m}$ or $TR^{(2)}_{2,m}$ – exhibited, within the experimental uncertainty, similar values of relative frequency shift.

Figure 4 shows the temporal evolution of the relative frequency shift, $\Delta\Omega/\Omega$, of a representative dilatational-like mode and a shear-like mode during the loading and outdiffusion phases, for H_2 and D_2. The relative frequency shift was calculated by taking the frequency of the peak with the fiber in air (room pressure) as the reference frequency. The best fits of an exponential function to the experimental data are included. Noticeable differences in the dynamic response of modes of the same subtype were not observed.

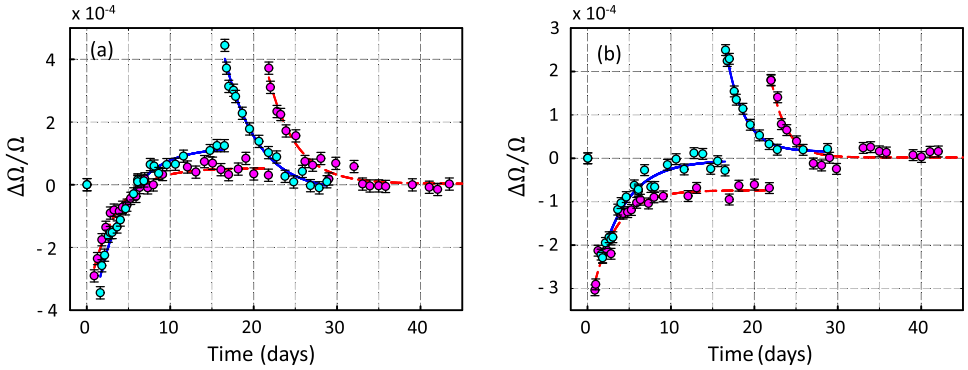

Fig. 4. Dynamic evolution of the relative frequency shift due to diffusion and outdiffusion of H_2 (blue dots) and D_2 (pink dots) for selected torsional-radial modes: (a) $TR^{(2)}_{2,6}$ and (b) $TR^{(1)}_{2,8}$. Lines show the best fit.

A thorough examination of the sources of error in the experimental data was conducted. Uncertainty in temperature and pressure during the experiment were by far the main sources of error. Considering the temperature coefficients [18], an uncertainty in temperature of 0.1 °C

Optics EXPRESS

results in an uncertainty of 0.06×10^{-4} and 0.1×10^{-4} in the relative frequency shift for $TR^{(1)}_{2,m}$ and $TR^{(2)}_{2,m}$ modes, respectively. The pressure uncertainty of 0.3 bar leads to uncertainties of 0.018×10^{-4} and 0.024×10^{-4} in the relative frequency shift. This calculation is based on the frequency shift experienced by the peak when the pressure was applied.

5. Discussion

The positive frequency shift with hydrogen and deuterium diffusion (negative shift in the outdiffusion stage) observed in both types of acoustic modes indicates that the two acoustic velocities increase with the presence of both gases. According to Eq. (5), this result implies that the main contribution comes from the change in Young's modulus, which is consistent with previous reports [10]. For both gases, the relative frequency shift is larger for dilatational-like acoustic modes. This can be explained by taking into account Eq. (5). The last term in Eq. (5) that accounts for the change in Poisson's ratio is negative for shear-like modes and positive for dilatation-like modes. As the other terms are common to both types of modes, this contribution counteracts the effect of Young's modulus in the first case and adds up in the second. Furthermore, a larger shift is achieved with H_2 compared to D_2, for both types of acoustic modes.

Table 1 summarizes the change in the relative frequencies of the saturated fiber once gas pressure was released, compared to the original fiber. The included values are the result of averaging the relative frequency shift at saturation of all modes measured for each sub-type. The uncertainties stated include frequency errors resulting from the PSD fitting process and the temperature and pressure uncertainty contribution.

Table 1. Relative frequency shift at saturation and time constant

	$\Delta\Omega/\Omega$		$t_{95\%}$ (days)	
Gas type	$TR^{(1)}_{2,m}$	$TR^{(2)}_{2,m}$	Loading	Outdiffusion
H_2	$(2.6 \pm 0.1) \times 10^{-4}$	$(4.1 \pm 0.2) \times 10^{-4}$	10.4 ± 1.2	9.2 ± 1.2
D_2	$(1.9 \pm 0.1) \times 10^{-4}$	$(3.7 \pm 0.1) \times 10^{-4}$	8.0 ± 1.2	9.1 ± 1.2

The experimental time constants for gas loading and outdiffusion phases were obtained from exponential fits of the dynamic curves. The time interval that takes the dynamic response to reach 95% of the steady state, $t_{95\%}$, is shown in Table 1. These values are the average over all measured modes. In all cases, the uncertainty is < 1.2 days. Notice that the time constants during the loading and outdiffusion stages are comparable when considering the uncertainty. The time constant values obtained by this method range between 8.0 days and 10.4 days. Those values are somehow comparable to those reported in other works. For example, following the approach described in [24], $t_{95\%}$=11.6 days is expected for the H_2 loading in a 125 μm diameter fiber at 23°C. In [31], experimental measurements on different types of fibers were performed and $t_{95\%}$=8.3 days were found for GeO_2 doped core single-mode fiber at room temperature. In [33], $t_{95\%}$=11.6 days was measured for H_2 fiber outdiffusion.

The increase in the two acoustic velocities can be calculated from the relative frequency shifts by taking into account Eq. (1) and (2). The increase in the two acoustic velocities Δv_S and Δv_L at saturation is shown in Table 2. The acoustic velocities of the pristine fiber assumed for this calculation were 3740 m/s and 5996 m/s, respectively [20], and changes in the fiber radius were neglected. The change in the two velocities is slightly smaller in the D_2 loaded fiber than in the H_2 loaded fiber. We attribute the differences in the elastic response to the different molecular mass of H_2 and D_2. The increase in longitudinal acoustic velocity aligns with previous reports. In [28], an increase of ~2.5 m/s was reported when experimental conditions were similar to ours.

As mentioned previously, among the different contributions to the frequency shift described in Eq. (5), the change in Poisson's ratio is the only one that differs between the two subtypes

Optics EXPRESS

Table 2. Increment of acoustic velocities and Poisson's ratio at saturation

Gas type	$\Delta v_S\ (m/s)$	$\Delta v_L\ (m/s)$	$\Delta\nu$
H_2	(0.96 ± 0.04)	(2.46 ± 0.12)	$(1.6 \pm 0.3) \times 10^{-4}$
D_2	(0.71 ± 0.04)	(2.23 ± 0.04)	$(1.9 \pm 0.2) \times 10^{-4}$

of acoustic modes. Therefore, the increase in Poisson's ratio due to the presence of gas in the fiber can be calculated from the difference between the relative frequency shift of $TR^{(1)}_{2,m}$ and $TR^{(2)}_{2,m}$ modes. Table 2 shows the increase in the Poisson's ratio at saturation. This increase was obtained using the relative frequency changes at saturation shown in Table 1 and assuming a value of $\nu = 0.174$ for silica. The change of Poisson's ratio can also be obtained from the two acoustic velocities, as it is solely dependent on the ratio between them [29].

It is important to note that the diffusion dynamics and saturation concentration of the gas in the fiber depend on temperature and pressure [25]. Therefore, the acoustic velocities and Poisson's ratio changes that are summarized in Table 2 are only applicable to the conditions of the experiments.

The present method demonstrates that the FSBS can detect changes in the elastic properties of the fiber immediately after the onset of gas loading (see Fig. 4). In most methods based on absorption [2,7,24,31], refractive index change [25,32] or backward Brillouin scattering [28], there is a lag time before the effects of gas diffusion are detected. These methods are sensitive to changes in the fiber core, thus, the gas must reach the fiber core to be able to detect its effects. Under the experimental conditions of this work, modelling of the diffusion dynamics of hydrogen into the optical fiber [25] indicates that it takes over 24 hours for the concentration of hydrogen in the core area to become noticeable. Conversely, FSBS enables detection of changes at any point of the optical fiber cross-section, including near the surface, as the displacement field of FSBS acoustic modes overlaps the entire fiber cross-section.

A comparative of the performance of the present work based on FSBS and other different methods presented in the literature to detect hydrogen diffusion in optical fibers is given in Table 3. Optical methods that are based on interrogating the changes of refractive index or optical absorption in the fiber core due to hydrogen diffusion [24,25,27] exhibit very low detection limit, in the order of 1 ppm or lower. The detection limit demonstrated by using BBS is limited by the low sensitivity (1 MHz/ppm) and the linewidth of the Brillouin gain line. In this regard, FSBS takes advantage of the narrow linewidth of the gain peaks and the multi-peak response, both of which contribute to reduce uncertainty, thereby enhancing the detection limit.

Table 3. Comparison of performance of different methods for monitoring H_2 diffusion in optical fibers

Ref. / Measuring technique	Detection limit (ppm)	Spatial resolution	Response time (hours)
Present work / FSBS	90	25 cm	< 0.1
[24] / Optical absorption	1[b]	1 km	> 24[a]
[25] / FBG Fabry–Perot interferometry	10	10 mm	> 24[a]
[27] / CP-ϕOTDR	< 1	6 m	> 24[a]
[8] / BBS	950	2.5 m	> 24[a]

[a]Estimated value at 23°C and 50 bar.
[b]A detection limit for attenuation changes of 0.1 dB/km is assumed.

Optics EXPRESS

6. Conclusions

Forward-stimulated Brillouin scattering is proposed as a direct technique for monitoring the temporal dynamics of hydrogen and deuterium diffusion in standard single-mode optical fibers. The proposed method is based on the dependence of the cutoff frequency of FSBS acoustic modes on the mechanical properties of the fiber. Thus, changes in the elastic properties of the fiber due to gas diffusion were accurately determined by measuring the frequency of a set of specific FSBS acoustic modes. By taking advantage of the different characteristics of the two sub-types of torsional-radial acoustic modes, changes in the two acoustic velocities and in the Poisson's ratio produced in H_2 / D_2 loaded optical fiber were determined. Additional distinctive features that may support potential uses of FSBS include the ability to detect changes in the fiber from the gas onset and the relatively short fiber section (cm scale) required.

Funding. Ministerio de Ciencia, Innovación y Universidades (PID2023-146725OB-I00, CNS2023-145717); Generalitat Valenciana (CIPROM/2022/30); Horizon 2020 Framework Programme (H2020-MSCA-RISE-2019-872049).

Disclosures. The authors declare no conflicts of interest.

Data availability. Data underlying the results presented in this paper are not publicly available at this time but may be obtained from the authors upon reasonable request.

References

1. J. Stone, "Interactions of hydrogen and deuterium with silica optical fibers: A review," J. Lightwave Technol. **5**(5), 712–733 (1987).
2. J. Stone, A. R. Chraplyvy, J. M. Wiesenfeld, *et al.*, "Overtone absorption and Raman spectra of H_2 and D_2 in silica optical fibers," AT&T Bell Lab. Technical J. **63**(6), 991–1000 (1984).
3. J. E. Shelby, "Molecular diffusion and solubility of hydrogen isotopes in vitreous silica," J. Appl. Phys. **48**(8), 3387–3394 (1977).
4. C. M. Hartwig and J. Vitko, "Raman spectroscopy of molecular hydrogen and deuterium dissolved in vitreous silica," Phys. Rev. B **18**(7), 3006–3014 (1978).
5. A. P. Bazakutsa, O. Butov, and K. Golant, "Influence of hydrogen loading on active fibers," *Optical Fiber Communication Conference and Exposition and the National Fiber Optic Engineers Conference* (2013).
6. C. Martelli, A. L. C. Triques, A. Braga, *et al.*, "Operation of optical fiber sensors in hydrogen-rich atmosphere," Proc. SPIE **7653**, 765326 (2010).
7. S. Delepine-Lesoille, X. Pheron, J. Bertrand, *et al.*, "Industrial qualification process for optical fibers distributed strain and temperature sensing in nuclear waste repositories," J. Sensors **2012**(1), 369375 (2012).
8. S. Delepine-Lesoille, J. Bertrand, L. Lablonde, *et al.*, "Distributed hydrogen sensing with Brillouin scattering in optical fibers," IEEE Photonics Technol. Lett. **24**(17), 1475–1477 (2012).
9. S. Leparmentier, J. L. Auguste, G. Humbert, *et al.*, "Study of the hydrogen influence on the acoustic velocity of single-mode fibers by Rayleigh and Brillouin backscattering measurements," Proc. SPIE **9634**, 963432 (2015).
10. F. Kong and L. Dong, "Precise tailoring of acoustic velocity in optical fibers by hydrogenation and uv exposure," Opt. Express **20**(25), 27810–27819 (2012).
11. P. J. Lemaire, R. M. Atkins, V. Mizrahi, *et al.*, "High pressure H_2 loading as a technique for achieving ultrahigh uv photosensitivity and thermal sensitivity in geo doped optical fibres," Electron. Lett. **29**(13), 1191–1193 (1993).
12. C. L. Liou, L. A. Wang, M. C. Shih, *et al.*, "Characteristics of hydrogenated fiber Bragg gratings," Appl. Phys. A **64**(2), 191–197 (1997).
13. A. Zadok, H. H. Diamandi, Y. London, *et al.*, "*Forward Brillouin Scattering in Standard Optical Fibers: Single-Mode, Polarization-Maintaining, and Multi-Core*," *Springer Series in Optical Sciences* (Springer, 2022), Vol. 240.
14. Y. London, H. H. Diamandi, and A. Zadok, "Electro-opto-mechanical radio-frequency oscillator driven by guided acoustic waves in standard single-mode fiber," Appl. Phys. Lett. **2**(4), 041303 (2017).
15. G. Bashan, H. H. Diamandi, E. Zehavi, *et al.*, "A forward Brillouin fibre laser," Nat. Commun. **13**(1), 3554 (2022).
16. Y. Liu, Y. Ning, P. Chen, *et al.*, "Narrow linewidth all-optical optomechanically microwave oscillator based on forward stimulated Brillouin scattering," J. Lightwave Technol. **41**(16), 5303–5309 (2023).
17. Y. Antman, A. Clain, Y. London, *et al.*, "Optomechanical sensing of liquids outside standard fibers using forward stimulated Brillouin scattering," Optica **3**(5), 510–516 (2016).
18. L. A. Sánchez, A. Díez, J. L. Cruz, *et al.*, "Strain and temperature measurement discrimination with forward Brillouin scattering in optical fibers," Opt. Express **30**(9), 14384–14392 (2022).
19. X. Li, Y. Lu, and Z. Zhang, "Simultaneous measurement of temperature and pressure based on forward Brillouin scattering in double-coated optical fiber," J. Lightwave Technol. **41**(15), 5130–5137 (2023).
20. L. A. Sánchez, A. Díez, J. L. Cruz, *et al.*, "High accuracy measurement of Poisson's ratio of optical fibers and its temperature dependence using forward-stimulated Brillouin scattering," Opt. Express **30**(1), 42–52 (2022).

Optics EXPRESS

21. H. H. Diamandi, Y. London, G. Bashan, *et al.*, "Forward stimulated Brillouin scattering analysis of optical fibers coatings," J. Lightwave Technol. **39**(6), 1800–1807 (2021).
22. Z. Hua, D. Ba, D. Zhou, *et al.*, "Nondestructive and distributed measurement of optical fiber diameter with nanometer resolution based on coherent forward stimulated Brillouin scattering," Light: Adv. Manufact. **2**(4), 1 (2021).
23. C. Álvarez-Ocampo, M. Delgado-Pinar, A. Díez, *et al.*, "Experimental study towards the development of highly sensitive opto-mechanical sensors based on FSBS in telecom optical fibers," Opt. Express **32**(23), 41984–41992 (2024).
24. P. J. Lemaire, "Reliability of optical fibers exposed to hydrogen: prediction of long-term loss increases," Opt. Eng. **30**(6), 780–789 (1991).
25. P. L. Swart, A. A. Chtcherbakov, W. L. Joubert, *et al.*, "Study of the pressure dependence of hydrogen diffusion in optical fiber by an interferometric technique," Opt. Commun. **217**(1-6), 189–196 (2003).
26. L. B. Fu, G. Tan, W. J. Xu, *et al.*, "Ultraviolet-initiated reactions of H_2 with germanosilicate fibers and H_2 concentration dependence of the Bragg wavelength of a fiber grating," Opt. Lett. **25**(8), 527–529 (2000).
27. A. García-Ruíz, A. Morana, L. Costa, *et al.*, "Distributed detection of hydrogen and deuterium diffusion into a singlemode optical fiber with chirped-pulse phase-sensitive optical time-domain reflectometry," Opt. Lett. **44**(21), 5286–5289 (2019).
28. A. Bernstein, E. Zehavi, Y. London, *et al.*, "Tensor characteristics of forward Brillouin sensors in bare and coated fibers," APL Photonics **8**(12), 126105 (2023).
29. A. D. Pierce, *Acoustics: An introduction to Its Physical Principles and Applications*, 3rd ed. (Springer, 2019).
30. L. A. Sánchez, A. Díez, J. L. Cruz, *et al.*, "Recent advances in forward Brillouin scattering: Sensor applications," Sensors **23**(1), 318 (2022).
31. E. Modone, G. Parisi, and B. Sordo, "Experimental determination of time constant for reversible diffusion of H_2 in optical fibers," J. Opt. Commun. **8**(3), 98–101 (1987).
32. D. E. Vogler, M. G. Müller, and M. W. Sigrist, "Fiber-optic cavity sensing of hydrogen diffusion," Appl. Opt. **42**(27), 5413–5417 (2003).